

1 **Research Article**

2 **Influencing mechanism of pre-existing nanoscale Al₅Fe₂ phase on Mg–Fe**
3 **interface in friction stir spot welded Al-free ZK60–Q235 joint**

4 R.Z. Xu ^{1,2}, Q. Yang ^{3,4}, D.R. Ni ¹, B.L. Xiao ¹, C.Z. Liu ², Z.Y. Ma ^{1,*}

5 ¹*Institute of Metal Research, Chinese Academy of Sciences, Shenyang 110016, China*

6 ²*College of Material Science and Engineering, Shenyang Aerospace University, Shenyang*
7 *110136, China*

8 ³*Department of Materials Science and Engineering, University of Illinois at*
9 *Urbana-Champaign, 1304 W Green St, Urbana, IL 61801, United States*

10 ⁴*Fredrick Seitz Materials Research Laboratory, University of Illinois at Urbana-Champaign,*
11 *104 S Goodwin Ave, Urbana, IL 61801, United States*

12 [Received 24 May 2019; Received in revised form 28 August 2019; Accepted 13 September 2019]

13 *Corresponding author. Prof.; Tel.: +86 24 83978908.

14 *E-mail address:* zyma@imr.ac.cn (Z.Y. Ma).

15 Al-free ZK60 magnesium (Mg) alloy sheet was selected as substrate material of
16 Mg–steel pinless friction stir spot welding (FSSW), avoiding the effect of the Al element in
17 the substrate on the alloying reaction of Mg-iron (Fe) interface. The sound FSSW joint of
18 ZK60 Mg alloy and Q235 steel with a hot-dipped aluminum (Al)-containing zinc (Zn) coating
19 was successfully realized. The detailed microstructural examinations proved that Al₅Fe₂ phase
20 at the Mg-Fe interface came from the pre-existing Al₅Fe₂ phase in the coating and acted as the
21 transition layer for promoting the metallurgical bonding of Mg and Fe. The interfaces with
22 well-matched lattice sites among Fe, Al₅Fe₂ and Mg were formed during FSSW. A low energy
23 interface with good match of lattice sites ((002)_{Al₅Fe₂}//(110)_{Fe}, [110]_{Al₅Fe₂}//[$\bar{1}$ 13]_{Fe}) between
24 Al₅Fe₂ and Fe was identified. For the interface between Al₅Fe₂ and Mg, an orientation

1 relationship of $(6\bar{2}2)_{\text{Al}_5\text{Fe}_2} // (3\bar{1}\bar{1}\bar{2})_{\text{Mg}}$ and $[1\bar{5}\bar{8}]_{\text{Al}_5\text{Fe}_2} // [2\bar{4}23]_{\text{Mg}}$ was observed. The
2 tensile–shear load of the ZK60–steel joint could reach 4.6 kN. Moreover, the joint fracture
3 occurred at the interface between the Al_5Fe_2 layer and the Mg alloy substrate, suggesting the
4 brittle fracture characteristic.

5 *Keywords:* Dissimilar welding; Friction stir spot welding; Magnesium alloys; steels; Zinc
6 coating

7 **1. Introduction**

8 The composite structure of ultra-light weight Mg alloys and steels prepared by various
9 welding techniques has been considered as a promising way to reduce vehicle weight and
10 save energy [1-5]. However, according to the Mg–Fe binary phase diagram, Mg and Fe are
11 immiscible [6]. Therefore, it is hard to achieve a metallurgical bonding between Mg and steel
12 directly [7,8]. It was reported that a metallurgical bonding between Mg alloy and steel could be
13 realized by the reaction between Al that diffused from the Mg alloy substrate and Fe to form
14 Al_5Fe_2 intermetallic compound (IMC) at the interface during welding [9-14]. Such bonding has
15 been successfully achieved by various welding techniques, including friction stir welding
16 (FSW) [9], resistance spot welding [10,11], laser welding [12,13] and laser-tungsten inert gas
17 hybrid welding [14].

18 It is a simple and effective way of utilizing the alloying elements from base metals to
19 modify the interfacial bonding of Mg–Fe [15]. However, such method limits obviously the type
20 of weldable Mg alloys, i.e. to the Al-containing Mg alloys. Furthermore, it increases the
21 difficulty of achieving sound welds, especially for welding methods with low process
22 temperature (such as ultrasonic spot welding (USW) and FSW [16-18]). The diffusion of Al to

1 the interface is limited during these welding processes.

2 Friction stir (spot) welding (FS(S)W) integrates the advantages of small thermal
3 deformation, sound mechanical properties and green welding process ^[19-22], and therefore has
4 a good potential in the welding of dissimilar metals ^[23,24]. However, it was reported that in the
5 AM60 (Mg-Al-Mn)-DP600 dual phase steel FSSW joint, there was no evidence of
6 intermetallic compound (IMC) formation, so only a mechanical bonding was formed between
7 Mg alloy and steel ^[25]. In addition, in the USWed AZ31B-steel joint without an interlayer, as
8 there was no reaction between Fe and Mg, no transitional zone formed at the interface of Mg
9 and steel ^[26]. To realize easily and reliably Mg-Fe interfacial metallurgical reaction, a novel,
10 simple and effective approach that could supply Al for the interfacial reaction of Mg and steel
11 is urgently needed.

12 Some studies thought that Al-containing Zn coating (0.1-0.3 wt% Al) could involve in
13 the interfacial reaction, forming the Fe-Al phase at the interface during the laser welding of
14 AZ31 Mg alloy and steel ^[27,28]. However, it was also reported that the Zn-Al coating was
15 completely squeezed out of bonded region during the joining process of Mg-Al-Zn alloys and
16 steel ^[15,19], so it did not contribute to the metallurgical bonding between Mg alloy and steel.

17 It should be pointed out that the influencing mechanism of Zn-Al coating on the
18 interfacial reaction between Al-containing Mg alloys and steels is difficultly elucidated
19 because both Mg alloy substrate and Zn coating contained Al element in above investigations.
20 In addition, although it was believed that the Al-Fe IMC played an important role in the
21 welding of Mg alloys to steels ^[9-18, 27,28], the bonding mechanism among the Mg alloy, Al-Fe
22 IMC and steel is not well understood.

1 In a previous study on FSSW of Al-containing AZ31 Mg alloy-steel, the present authors
2 suggested that the Al_5Fe_2 phase in the Al-containing Zn coating on the steel surface, formed
3 during the hot-dip galvanizing process, could promote the metallurgical bonding at the Mg-Fe
4 interface during the FSSW process [29]. However, the bonding mechanism among the Mg alloy,
5 Al-Fe IMC and steel has not been identified in Ref. 29.

6 In this study, an Al-free Mg alloy ZK60 was selected to replace the Al-containing Mg
7 alloy AZ31 as the Mg alloy substrate. ZK60 sheet and steel sheet with an Al-containing Zn
8 coating was welded by FSSW. The aim is to (a) further prove the role of Al source in the Zn
9 coating in the Mg-Fe joining and (b) elucidate the bonding mechanism among the Mg alloy,
10 Al-Fe IMC and steel.

11 **2. Experimental**

12 *2.1. Materials*

13 2.4 mm-thick ZK60 Mg alloy sheet with a composition of Mg-5.50Zn-0.04Zr (wt%)
14 and 1.5 mm-thick Q235 steel sheet with a composition of Fe-0.2C-0.40Mn-0.16Si (wt%)
15 were used in this study. The surface of the steel was hot-dipped with Al-containing Zn
16 coating.

17 *2.2. FSSW process*

18 ZK60 specimen was lapped on the top of Q235 steel specimen by a holding fixture. The
19 FSSW operation was conducted at a tool rotation rate of 3000 rpm and a plunge rate of 2.5
20 mm/s using a pinless welding tool 10 mm in shoulder diameter. The dwell time was 5 s and
21 the tool withdrawing rate was 30 mm/s at the end of each spot welding operation. The
22 presupposed plunge depth was 1.0 mm.

1 2.3. Temperature measurement

2 The temperature profile of the interface zone during FSSW was measured using a K-type
3 thermocouple 0.5 mm in diameter. Two cylindrical holes 0.8 mm in diameter was separately
4 machined in the steel sheet and the thermocouples were fastened at the top of the hole and the
5 interface between Mg alloy and steel by high temperature glue. The schematic of the location
6 of the temperature measurement is shown in Fig. 1.

7 2.4. Analysis methods

8 Specimens for microstructure examinations were sectioned through the center of the
9 joints and parallel to the loading direction. After being mechanically ground and polished, the
10 specimens were etched with an etching reagent consisting of 4.2 g picric acid, 10 ml acetic
11 acid, 10 ml H₂O, and 70 ml ethanol. Microstructures were examined by optical microscopy
12 (OM), scanning electron microscopy (SEM, LEO Supra 35) with energy dispersive
13 spectrometer (EDS), and transmission electron microscopy (TEM, JEOL 2010F).
14 Cross-sectional TEM specimens were prepared using focused ion beam/scanning electron
15 microscopy (FIB/SEM, FEI Helios 600i). The fuming HNO₃ etched coating surface with a
16 length of 5 mm and a width of 3 mm was analyzed by X-ray diffraction (XRD) using CuK_α
17 radiation ($\lambda = 1.5406 \text{ \AA}$) with 2θ in the range of 20° to 90° and a scan rate of 0.05°/min.

18 Lap-shear tensile specimens with a length of 100 mm, a width of 30 mm and an overlap
19 area of 30 mm × 30 mm were electrical discharge machined from the FSSW joint. Lap-shear
20 tensile test was conducted using a Zwick/Roell Z050 tester at a speed of 0.5 mm/min. The
21 load values for each condition were calculated by averaging three test results. The fracture
22 location and characteristics were examined by OM and SEM.

1 **3. Results**

2 *3.1. Characteristics of Zn-Al coated steel*

3 The SEM microstructure of Zn-Al coating surface is shown in Fig. 2(a). The chemical
4 composition of point B (Fig. 2(a)) is 97.25 wt% Zn, 2.14 wt% Fe and 0.61 wt% Al as shown
5 in Fig. 2(b), reflecting that the coating contained a small quantity of Al element beside Zn
6 element. It can be seen that the thickness of the coating was approximately 15 μm from Fig.
7 3(a). Line scan analysis of the coating showed in Fig. 3(a) indicated that an Al rich layer
8 formed at the interface between Zn coating and Fe. The Al rich layer was identified as Al_5Fe_2
9 IMC, as shown by XRD (Fig. 4).

10 From Figs. 3 and 4, it is clear that the interface between the coating and steel was
11 composed of ultra-thin Al_5Fe_2 IMC. The Al_5Fe_2 IMC was believed to form during the hot-dip
12 galvanizing process.

13 *3.2. Characteristics of FSSW ZK60–Q235 joint*

14 Fig. 5(a) shows a typical cross-sectional photograph of the FSSW ZK60–Q235 joint. A
15 shallow keyhole was detected on the Mg alloy sheet and a little flash appeared on its
16 periphery. It was clearly observed that a sound joint formed between ZK60 Mg alloy and
17 Q235 steel using pinless FSSW by the addition of Zn-Al coating.

18 The typical interfacial microstructure was further investigated as shown in Fig. 5(b)–(e).
19 It can be seen from Fig. 5(b) that a short Mg-Zn IMC layer, as identified in a previous study
20 ^[29], formed on the keyhole periphery, but a long crack appeared at the interface in this
21 reaction zone, lowering seriously its effective bonding area. However, ZK60 and Q235 were
22 bonded well under the pinless welding tool (Fig. 5(c)). The representative line analyses of Mg,

1 Fe, Zn and Al cross the interface for lines D and E between ZK60 and steel are respectively
2 shown in Fig. 5(d) and (e). It is indicated that Al was still rich at the interface between ZK60
3 and steel, but no significant Zn was found at the interface next to the steel side. The Al rich
4 layer was so thin that the EDS result was not accurate to reflect its thickness and composition.

5 The interface was further examined by TEM. Fig. 6(a) shows the high-angle annular dark
6 field-scanning tunneling electron microscopy (HAADF-STEM) image of the ZK60–steel
7 interface. An uniform and continuous ultra-thin layer about 150 nm in thickness was clearly
8 observed at the interface. Elemental mappings shown in Fig. 6(b) further revealed that this
9 layer was rich in Al. EDS analysis in Fig. 6(c) showed that the interface layer had a
10 composition of 70.2 at.% Al and 29.8 at.% Fe, close to that of Al_5Fe_2 IMC. Selected area
11 diffraction pattern (SADP) in Fig. 6(d) confirmed that this layer should be the orthorhombic
12 Al_5Fe_2 .

13 The orientation relationships (ORs) of the $\text{Al}_5\text{Fe}_2/\text{Fe}$ and $\text{Al}_5\text{Fe}_2/\text{Mg}$ heterophase interfaces
14 were determined by SADP, as shown in Fig. 7. The SADP in Fig. 7(a) was taken along the
15 zone axis of $[\bar{1}13]_{\text{Fe}}$ and $[110]_{\text{Al}_5\text{Fe}_2}$. The diffraction spot of $(110)_{\text{Fe}}$ was found to superimpose
16 on that of $(002)_{\text{Al}_5\text{Fe}_2}$, indicating that the OR between Fe and Al_5Fe_2 can be expressed as:
17 $(002)_{\text{Al}_5\text{Fe}_2} // (110)_{\text{Fe}}$, $[110]_{\text{Al}_5\text{Fe}_2} // [\bar{1}13]_{\text{Fe}}$. The SADP in Fig. 7(b) was taken along the zone axis
18 of $[\bar{1}58]_{\text{Al}_5\text{Fe}_2}$ and $[2\bar{4}23]_{\text{Mg}}$. The diffraction spot of $(6\bar{2}2)_{\text{Al}_5\text{Fe}_2}$ was found to superimpose on
19 that of $(3\bar{1}2\bar{2})_{\text{Mg}}$, suggesting that the OR between Mg and Al_5Fe_2 is $(6\bar{2}2)_{\text{Al}_5\text{Fe}_2} // (3\bar{1}2\bar{2})_{\text{Mg}}$ and
20 $[\bar{1}58]_{\text{Al}_5\text{Fe}_2} // [2\bar{4}23]_{\text{Mg}}$.

21 In short, the Al-free ZK60 Mg alloy and Zn-Al coated Q235 steel formed a metallurgical
22 bonding during pinless FSSW, and the IMC phase of the interfacial zone was Al_5Fe_2 which

1 had crystallographic ORs with both Mg and Fe.

2 *3.3. Mechanical property and fracture characteristic of Mg–steel joint*

3 The tensile-shear tests showed that the load of joint could reach 4.6 kN (Fig. 8). Fig. 9(a)
4 shows the typical fracture location of the FSSW ZK60–Q235 joint. The joint fractured along
5 the interface between ZK60 Mg alloy and steel. Fig. 9(b) and (c) shows respectively the SEM
6 macrograph of the fracture surface and the magnified image of region C in Fig. 9(b) of the
7 Mg–steel joint on the steel side. Fracture surface on the steel side was quite smooth,
8 suggesting the brittle fracture characteristic. EDS analysis revealed that region D in Fig. 9(c)
9 consisted of 25.6 at.% Al, 72.3 at.% Fe and 2.1 at.% Zn (Fig. 9(d)) and region E in Fig. 9(c)
10 consisted of 45.1 at.% Al, 52.4 at.% Fe and 2.5 at.% Zn (Fig. 9(e)). Because this IMC layer
11 was extremely thin and the EDS X-rays were generated in a region a few micrometers in
12 depth, the percentage of Al determined by EDS was actually lower than that of the Al-Fe. This
13 result could further confirm that the Al rich layer was Al-Fe IMC. The fracture characteristic
14 shows that the interface between the Mg alloy and Al-Fe IMC was the weakest region of the
15 joint.

16 **4. Discussion**

17 *4.1. The role of Zn-Al coating in the FSSW process*

18 During the FSSW process, the action of rotation, plunge and dwelling of the stirring tool
19 supplied the pressure, reaction temperature and time for the metal in the lap interface. The
20 temperature of the interface between Mg alloy and steel was measured to be as high as 420 °C
21 (Fig. 10), which could melt the Zn coating with a melting point of 419.5 °C. Therefore, high
22 temperature and high pressure resulted in the melting of Zn coating, and destroyed oxide

1 films on the surfaces of both sheets ^[17,18]. A small amount of Zn diffused into Mg alloy base
2 (Fig. 5(c) and (e)), but the majority was squeezed out from the weld center, which spread
3 along the interface till piled into the edge zone of joint, forming the Mg-Zn IMC (Fig. 5(b)
4 and (d)) ^[29]. Thus, the fresh interfaces were exposed and tightly bonded after the Zn-Al
5 coating was pushed out. Obviously, the presence of Zn coating significantly improved the
6 weldability of Mg alloy and steel ^[17].

7 Al-Fe IMC played an important role in the bonding of Mg alloy and steel during FS(S)W
8 according to the present results (Figs. 5 and 6) and previous reports ^[9–18,27–31]. In previous
9 studies, it was believed that the Al-Fe IMC had a supply of Al from Mg-Al-Zn alloy. In fact,
10 in our previous work, Al₅Fe₂ phase had been detected at the Mg-Fe interface in the FSSW
11 AZ31-steel joint ^[29]. However, because there was Al element in both the AZ31 Mg alloy and
12 Zn-Al coating on the steel surface, the Al source at the interface was difficult to fully verify in
13 the FSSW AZ31-steel joint. Different significantly from our previous study, there was no Al
14 in ZK60 Mg alloy in this study, so Fe-Al IMC at the Mg-Fe interface was unambiguously
15 confirmed to come from the Zn-Al coating, and was not related to the Mg alloy substrate.

16 In the hot-dipped galvanization process, a small quantity of Al was added to the coating to
17 increase the brightness and improve the adhesion of Zn coating ^[32]. This resulted in the
18 formation of nanoscale Al₅Fe₂ due to the reaction between Al and Fe (Figs. 3 and 4). During
19 FSSW, the Al₅Fe₂ remained between the Mg alloy and steel substrates because of its high
20 melting point (1169 °C), and acted as an interlayer to promote metallurgical bonding at the
21 interface. In other words, the pre-existing Al₅Fe₂ phase played a key role in joining Mg alloy
22 to steel.

1 For the fusion welding of Mg-steel, adding a metal layer, such as Al, Ni, Cu and Cu-Zn
2 foil, was a common method [33,34]. The molten metal layer could improve the wettability
3 between Mg alloy and steel and promote their metallurgical bonding. In addition, in the
4 resistance spot welding (RSW) of AZ31 and steel, a nanoscaled Fe₂Al₅ transition layer was
5 coated onto the Fe surface using hot-dipped galvanization process, and subsequently, the Zn
6 coating was removed and the Fe₂Al₅ layer remained before welding. At last, AZ31 and steel
7 was welded by RSW with the assistance of Fe₂Al₅ layer [35]. Different from the fusion welding,
8 FSSW is a solid state joining method, so the interfacial reaction temperature is very low.
9 Therefore, the molten Zn coating improved the interfacial wettability of Mg alloy and steel,
10 which was the prerequisite for the effective welding between Mg alloy and steel in the solid
11 welding with a low temperature.

12 In short, the Zn-Al coating could play a dual role in joining Mg alloy and steel during
13 FSSW. On the one hand, it improved the interfacial wettability of Mg and steel significantly.
14 On the other hand, the pre-existing Al₅Fe₂ phase promoted the metallurgical joining of Mg
15 alloy and steel. In other words, it would be a novel and effective way of employing the
16 alloying element for the interfacial reaction of Mg/Fe by a hot-dipped Al-containing Zn
17 coating, making it possible to weld Al-free Mg alloys and steels.

18 *4.2. Bonding mechanism of Fe-IMC-Mg interface*

19 In a previous study [30], it was reported that the Fe-Al IMC could directly nucleate on
20 ferrite grains in the hot dip galvanizing process, forming Al₅Fe₂, which had well-defined ORs
21 with Fe substrate, such as [110]_{Al₅Fe₂}//[111]_{Fe}, (001)_{Al₅Fe₂}//(0 $\bar{1}$ 1)_{Fe} and ($\bar{1}$ 10)_{Al₅Fe₂}//(2 $\bar{1}$ 1)_{Fe}. As
22 shown in Fig. 7(a), an OR of (002)_{Al₅Fe₂}//(110)_{Fe} and [110]_{Al₅Fe₂}//[$\bar{1}$ 13]_{Fe} was identified for the

1 interface between Al_5Fe_2 and Fe in this study, and this OR is suggested to result in a
 2 low-energy interface ^[35]. Therefore, steel and Al_5Fe_2 IMC could bond very well.

3 For the interface between the pre-existing Al_5Fe_2 and Mg, an OR of $(\bar{6}\bar{2}\bar{2})_{\text{Al}_5\text{Fe}_2}/(3\bar{1}\bar{2}\bar{2})_{\text{Mg}}$
 4 and $[1\bar{5}\bar{8}]_{\text{Al}_5\text{Fe}_2}/[2\bar{4}23]_{\text{Mg}}$ was detected (Fig. 7(b)), indicating the formation of a
 5 metallurgically bonded interface. Theoretically, there may be other ORs between Al_5Fe_2 and
 6 Mg. Based on the lattice parameters $a = 0.7649$ nm, $b = 0.6413$ nm and $c = 0.4217$ nm for the
 7 orthorhombic Al_5Fe_2 and $a = 0.3209$ nm and $c = 0.5211$ nm for hexagonal close-packed Mg,
 8 some of the possible matching planes and matching directions of Al_5Fe_2 and Mg are shown in
 9 Table 1 besides our finding. The interplanar and interatomic misfits (δ) for this system are
 10 calculated by:

$$11 \quad \delta = \frac{2|d_{\text{Al}_5\text{Fe}_2} - d_{\text{Mg}}|}{(d_{\text{Al}_5\text{Fe}_2} + d_{\text{Mg}})} \times 100\% \quad (1)$$

12 where $d_{\text{Al}_5\text{Fe}_2}$ and d_{Mg} are the interplanar or interatomic distances of Al_5Fe_2 and Mg,
 13 respectively.

14 According to Table 1, the OR of $(\bar{6}\bar{2}\bar{2})_{\text{Al}_5\text{Fe}_2}/(3\bar{1}\bar{2}\bar{2})_{\text{Mg}}$ yields a mismatch of 6%, however,
 15 the $[1\bar{5}\bar{8}]_{\text{Al}_5\text{Fe}_2}/[2\bar{4}23]_{\text{Mg}}$ direction resulted in a large mismatch of 38%. On the other hand,
 16 Table 1 shows that the interplanar mismatching of $(021)_{\text{Al}_5\text{Fe}_2}/(0002)_{\text{Mg}}$ and $(002)_{\text{Al}_5\text{Fe}_2}/(01\bar{1}$
 17 $\bar{2})_{\text{Mg}}$ are both small, and the mismatching of $[0\bar{1}0]_{\text{Al}_5\text{Fe}_2}/[4\bar{2}\bar{2}0]_{\text{Mg}}$ and $[1\bar{1}\bar{2}]_{\text{Al}_5\text{Fe}_2}/[4\bar{2}\bar{2}0]_{\text{Mg}}$
 18 directions are also small.

19 In our previous study on the FSSW AZ31-steel joint ^[29], the Al_5Fe_2 phase in the Mg-Fe
 20 interface was suggested to originate from in the Al-containing Zn coating on the steel surface,
 21 and to promote the interfacial metallurgical bonding, however, the interface bonding
 22 mechanism has not been identified. In this study, the bonding mechanism at the interface

1 among the Fe, Al₅Fe₂ and Mg was clearly clarified based on the HAADF-STEM examinations
2 and analyses. In short, the well-matched lattice sites among Fe, Al₅Fe₂ and Mg suggest that
3 Al₅Fe₂ could serve as a potential transition layer to realize the high-strength FSSW of Mg
4 alloys (both Al-free and Al-containing) to steels.

5 *4.3. Properties and fracture characteristics of the FSSW ZK60–Q235 joint*

6 The load of FSSW Al-free ZK60 and Q235 steel joint with a diameter of 10 mm could
7 reach 4.6 kN, and the joint strength was about 59 MPa. In the AZ31-steel spot welded joint by
8 cold metal transfer (CMT) method, the maximum load of the joint with a diameter of 9 mm
9 was about 3 kN (~47 MPa joint strength) [36]. In addition, the strengths of the USW Mg-steel
10 joints with and without the addition of the Sn layer were about 45 MPa and 54 MPa,
11 respectively [26]. In the RSW Mg-steel joint, the joint load was in the range of 4.6-5 kN (about
12 10 mm in diameter) [35,37]. Clearly, the load of the present FSSW ZK60–Q235 joint was
13 superior or similar to that of the Mg-steel joints prepared by other welding techniques.

14 For the FSSW ZK60–Q235 joint, a small bonding zone formed at edge of the joint, but
15 there was a long crack at the interface, so the real contact area of the bonding interface in this
16 zone was small (Fig. 5(a)-(c)). In addition, Zn could not react directly with steel substrate due
17 to the separation of Fe-Al phase, and deformation of Mg substrate further enhanced the
18 generation and expansion of cracks, resulting in the weak joint between the reaction layer and
19 steel substrate [29]. Therefore, during tensile-shear testing the crack initiated at this bonding
20 interface. Subsequently, the crack propagated along the weak bonding interface. At last, the
21 joint fractured at the Mg-Al₅Fe₂ interface. Therefore, if there was no the adverse effects of the
22 deformation of the Mg sheet, the joint strength would be even higher.

1 Based on the above analyses, the pre-existing ultra-thin Al_5Fe_2 IMC played a key role in
2 joining Mg alloy and steel. Besides the large bonding area, there was a high bonding strength
3 among Mg, Al_5Fe_2 and steel due to the formation of metallurgical bonding as shown in Figs.
4 5-7. To aid the following discussion a schematic diagram is presented in Fig. 11. First, the
5 Zn-Al coating on the steel surface was melted due to the thermo-mechanical action of stirring
6 tool as shown in Fig. 11(a). Second, a small amount of Zn diffused into the Mg substrate, and
7 the majority of Zn was squeezed out of bonded region to the edge of the joint as shown in Fig.
8 11(a), (b) and (d). The crack was easily formed due to the slight deformation of Mg alloy
9 substrate and low strength between Mg-Zn IMC and Al_5Fe_2 (Fig. 11(b)).

10 Because the heat input was relatively low during the FSSW process, the Al-Fe phase
11 which had a well-defined orientation relationship with Fe remained after FSSW due to its
12 high melting point (Fig. 11(d)). Subsequently, Al_5Fe_2 as a transition layer formed a
13 heterophase interface with the Mg substrate (Fig. 11(f)). During tensile-shear test, the crack
14 initiated at the edge zone of the joint. After initiation, the crack propagated along the interface
15 between Mg and Al_5Fe_2 phase and resulted in failure at this interface (Fig. 11(c)).

16 **5. Conclusions**

17 In this study, Al-free ZK60 Mg alloy sheet and Zn-Al coated Q235 steel sheet was
18 welded by FSSW, and the bonding mechanism among Mg- Al_5Fe_2 -Fe was investigated. The
19 following conclusions are drawn.

20 (1) The sound FSSW joint of ZK60 Mg alloy and Q235 steel was successfully realized
21 with Al_5Fe_2 phase as the transition layer for promoting the metallurgical bonding of Mg-steel.
22 The adoption of Al-free Mg alloy substrate further proved that the Al_5Fe_2 phase at the Mg-Fe

1 interface came from the pre-existing Al_5Fe_2 phase in the coating.

2 (2) The interfaces with well-matched lattice sites among Fe, Al_5Fe_2 and Mg were formed
3 during FSSW. A low energy interface with good match of lattice sites ($(002)_{\text{Al}_5\text{Fe}_2} // (110)_{\text{Fe}}$,
4 $[110]_{\text{Al}_5\text{Fe}_2} // [\bar{1}13]_{\text{Fe}}$) was identified between Al_5Fe_2 and Fe. For the interface between Al_5Fe_2
5 and Mg, an orientation relationship of $(6\bar{2}2)_{\text{Al}_5\text{Fe}_2} // (3\bar{1}\bar{1}\bar{2})_{\text{Mg}}$ and $[\bar{1}5\bar{8}]_{\text{Al}_5\text{Fe}_2} // [\bar{2}4\bar{2}3]_{\text{Mg}}$ was
6 observed.

7 (3) The tensile-shear load of FSSW ZK60-steel joint could reach 4.6 kN, which was
8 superior or equivalent to that of the Mg-steel joints obtained by CMT, USW, or RSW
9 techniques. The joint fracture occurred at the interface between the Al_5Fe_2 layer and the Mg
10 alloy substrate, presenting the brittle fracture characteristic.

11 **Acknowledgements**

12 This work was supported financially by the National Natural Science Foundation of
13 China (Nos. 51601121, 51371179 and 51331008). Electron microscopy experiments were
14 carried out at the Center for Microanalysis of Materials at the Frederick Seitz Materials
15 Research Laboratory of University of Illinois at Urbana-Champaign, and supported by DOE
16 BES (No. DEFG02-01ER45923).

17 **Data availability**

18 The research data has been uploaded to Mendeley Data.

19 **References**

- 20 [1] R. Qiu, C. Iwamoto, S. Satonaka, J. Mater. Process. Technol. 209 (2009) 4186–4193.
21 [2] M. Elthalabawy, I.K. Tahir, Mater. Charact. 61 (2010) 703–712.
22 [3] W. Xu, D.L. Chen, L. Liu, H. Mori, Y. Zhou, Mater. Sci. Eng. A 537 (2012) 11–24.

- 1 [4] G. Song, T.T. Li, J.Y. Chi, L.M. Liu, *Scr. Mater.* 157 (2018) 10-14.
- 2 [5] G. Song, J.W. Yu, T.T. Li, J.F. Wang, L.M. Liu, *J. Manuf. Process.* 31 (2018) 131-138.
- 3 [6] A.A. Nayeb-Hashemi, J.B. Clark, L.J. Swartzendruber, *Binary Alloy Phase Diagram*,
- 4 ASM international, Materials Park, OH, 1990, p. 1722.
- 5 [7] H. Wang, G. Song, *Int. J. Precis. Eng. Manuf.* 17 (2016) 823–827.
- 6 [8] G. Song, T. Li, Z. Zhang, L. Liu, *J. Manuf. Process.* 30 (2017) 299–302.
- 7 [9] Y.C. Chen, K. Nakata, *Mater. Des.* 30 (2009) 3913–3919.
- 8 [10] L. Liu, L. Xiao, J.C. Feng, Y.H. Tian, S.Q. Zhou, Y. Zhou, *Metall. Mater. Trans. A* 41
- 9 (2010) 2651–2661.
- 10 [11] L. Liu, L. Xiao, D.L. Chen, J.C. Feng, S. Kim, Y. Zhou, *Mater. Des.* 45 (2013) 336–342.
- 11 [12] Y. Miao, D. Han, J. Yao, F. Li, *Mater. Des.* 31 (2010) 3121–3126.
- 12 [13] M. Wahba, S. Katayam, *Mater. Des.* 35 (2012) 701–706.
- 13 [14] C. Tan, L. Li, Y. Chen, W. Guo, *Mater. Des.* 49 (2013) 766–773.
- 14 [15] L.Q. Li, C.W. Tan, Y.B. Chen, W. Guo, F. Song, *Mater. Des.* 43 (2013) 59–65.
- 15 [16] C. Schneider, T. Weinberger, J. Inoue, T. Koseki, N. Enzinger, *Sci. Technol. Weld. Join.*
- 16 16 (2011) 100–106.
- 17 [17] Y.C. Chen, K. Nakata, *Mater. Des.* 30 (2009) 3913–3919.
- 18 [18] Y.C. Chen, K. Nakata, *Mater. Trans.* 50 (2009) 2598–2603.
- 19 [19] Y.Q. Mao, L.M. Ke, Y. Chen, F.C. Liu, X. Li, *J. Mater. Sci. Technol.* 34 (2008) 228–236.
- 20 [20] C.Y. Liu, B. Qu, P. Xue, Z.Y. Ma, K. Luo, M.Z. Ma, R.P. Liu, *J. Mater. Sci. Technol.* 4
- 21 (2018) 112–118.
- 22 [21] L.H. Wu, X.B. Hu, X.X. Zhang, Y. Li, Z.Y. Ma, X.H. Ma, B.L. Xiao, *Acta Mater.* 166

- 1 (2019) 371–385.
- 2 [22] R.Z. Xu, D.R. Ni, Q. Yang, C.Z. Liu, Z.Y. Ma, *J. Mater. Sci. Technol.* 32 (2016) 76–88.
- 3 [23] P. Xue, B.L. Xiao, Z.Y. Ma, *Metall. Mater. Trans. A* 46 (2015) 3091–3103.
- 4 [24] G.K. Padhy, C.S. Wu, S. Gao, *J. Mater. Sci. Technol.* 34 (2018) 1–38.
- 5 [25] T. Liyanage, J. Kilbourne, A.P. Gerlich, T.H. North, *Sci. Technol. Weld. Join.* 14 (2009)
- 6 500–508.
- 7 [26] V.K. Patel, D.L. Chen, S.D. Bhole, *Theo. Appl. Mech. Lett.* 14 (2014) 26–33.
- 8 [27] L.Q. Li, C.W. Tan, Y.B. Chen, W. Guo, C.X. Mei, *J. Mater. Process. Technol.* 213 (2013)
- 9 361–375.
- 10 [28] C.W. Tan, L.Q. Li, Y.B. Chen, C.X. Mei, W. Guo, *Int. J. Adv. Manuf. Technol.* 68 (2013)
- 11 1179–1188.
- 12 [29] R.Z. Xu, D.R. Ni, Q. Yang, B.L. Xiao, C.Z. Liu, Z.Y. Ma, *Mater. Charact.* 140 (2018)
- 13 197–206.
- 14 [30] Z.K. Zhang, X.J. Wang, P.C. Wang, G. Zhao, *Trans. Nonferrous Met. Soc. China* 24
- 15 (2014) 1709–1716.
- 16 [31] T. Liyanage, J. Kilbourne, A.P. Gerlich, T.H. North, *Sci. Technol. Weld. Join.* 24 (2009)
- 17 500–508.
- 18 [32] K.K. Wang, L.W. Chang, D.S. Gan, H.P. Wang, *Thin Solid Films* 518 (2010) 1935–1942.
- 19 [33] T.T. Li, G. Song, P.N. Yu, L.M. Liu, *Mater. Des.* 185 (2019) 107903.
- 20 [34] G. Song, T.T. L, L. Chen, *Mate. Sci. Eng. A* 736 (2018) 306–315.
- 21 [35] L. Liu, L. Xiao, J. Feng, L. Li, S. Esmacili, Y. Zhou, *Scr. Mater.* 65 (2011) 982–985.
- 22 [36] R. Cao, Q.W. Xu, H.X. Zhu, G.J. Mao, Q. Lin, P. Wang, *J. Manuf. Sci.* 139 (2017)

1 02100101–02100111.

2 [37]L. Liu, L. Xiao, J.C. Feng, Y.H. Tian, S.Q. Zhou, Y. Zhou, Metall. Mater. Trans. A 41

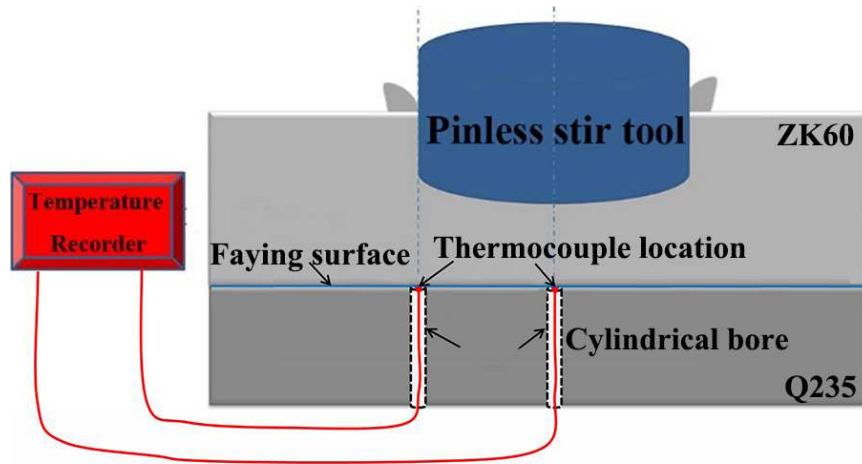
3 (2010) 2651–2661.

4

5 **Table 1** Possible matching planes and directions of Fe₂Al₅ and Mg in FSSW

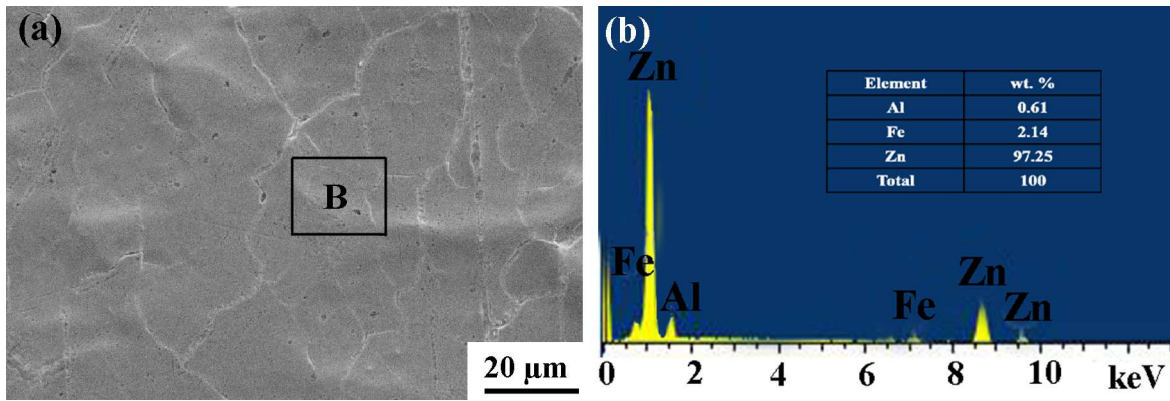
Matching planes or directions	(021) _{Al₅Fe₂} //(0002) _{Mg}	(002) _{Al₅Fe₂} //(01 $\bar{1}\bar{2}$) _{Mg}	(6 $\bar{2}\bar{2}$) _{Al₅Fe₂} //(3 $\bar{1}\bar{1}\bar{2}$) _{Mg}	[0 $\bar{1}\bar{0}$] _{Al₅Fe₂} //[4 $\bar{2}\bar{2}\bar{0}$] _{Mg}	[1 $\bar{1}\bar{2}$] _{Al₅Fe₂} //[4 $\bar{2}\bar{2}\bar{0}$] _{Mg}	[1 $\bar{5}\bar{8}$] _{Al₅Fe₂} //[2 $\bar{4}\bar{2}\bar{3}$] _{Mg}
$d_{Al_5Fe_2}$ (nm)	0.255	0.211	0.103	0.642	0.654	0.049
d_{Mg} (nm)	0.261	0.190	0.097	0.642	0.642	0.072
Mismatch (%)	2.3	10.5	6.0	0	1.9	38

6



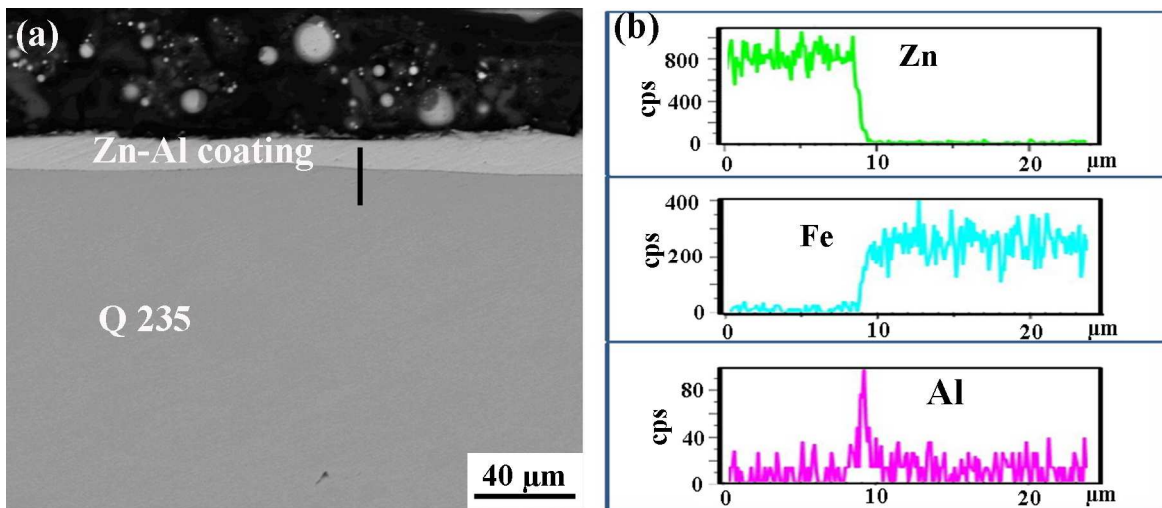
1
2

Fig. 1. Schematic of ZK60–steel FSSW and position of temperature measurement.



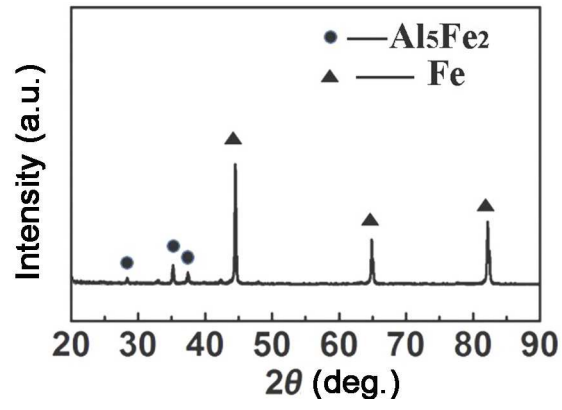
3
4
5

Fig. 2. (a) SEM micrograph of coating surface on Q235 steel and (b) EDS spectra obtained from zone B in Fig. 2(a).



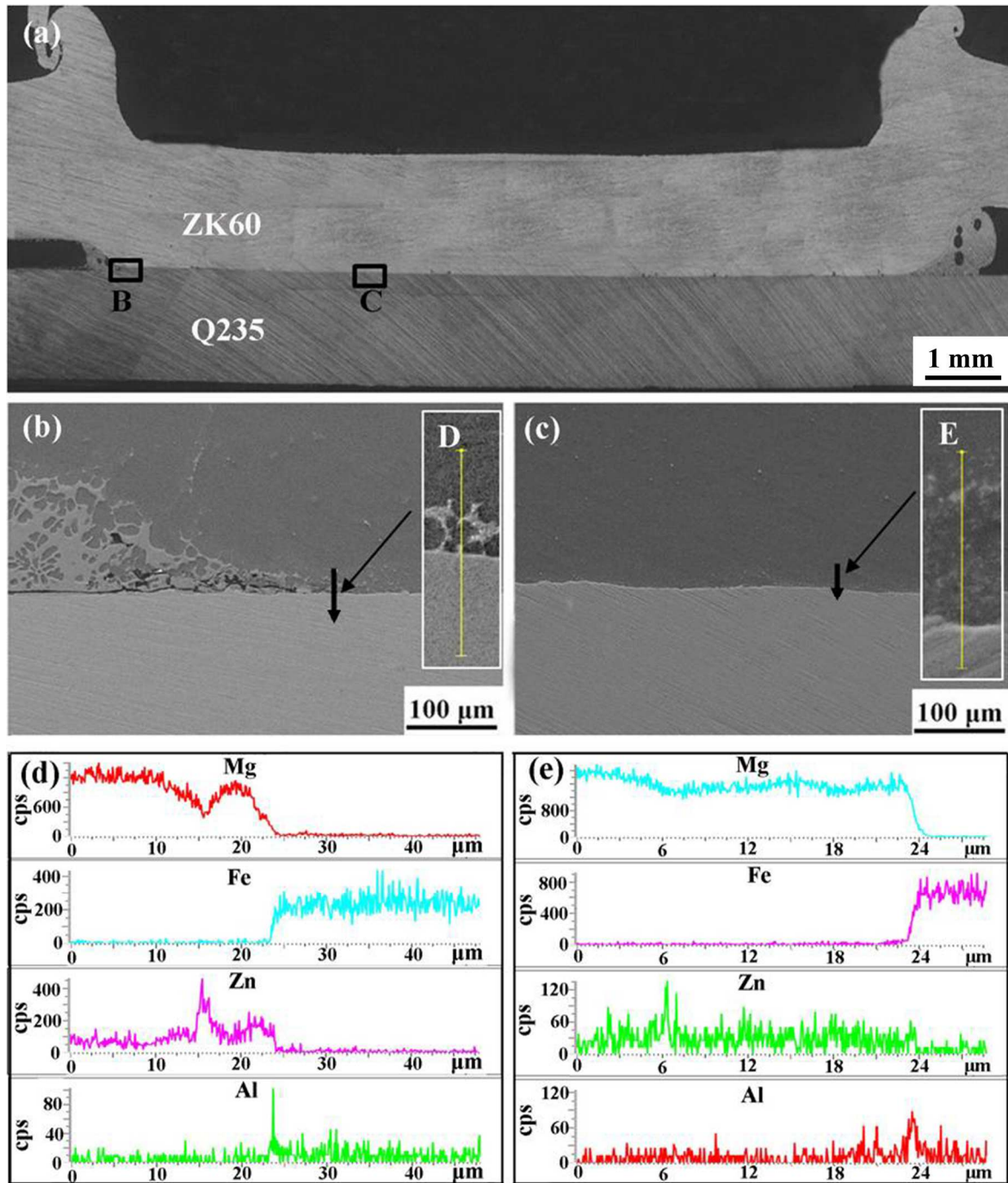
6
7
8

Fig. 3. (a) SEM micrograph of cross-sectioned Zn-Al coated steel and (b) elemental analysis of black line in Fig. 3(a).

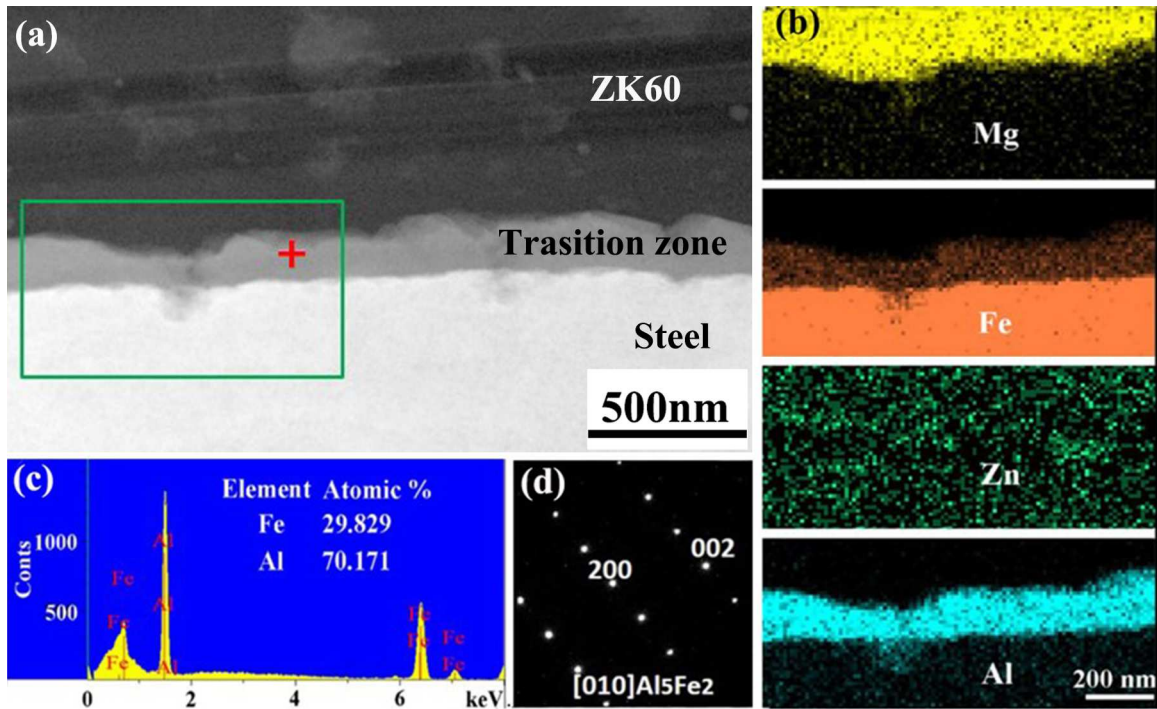


1
2
3

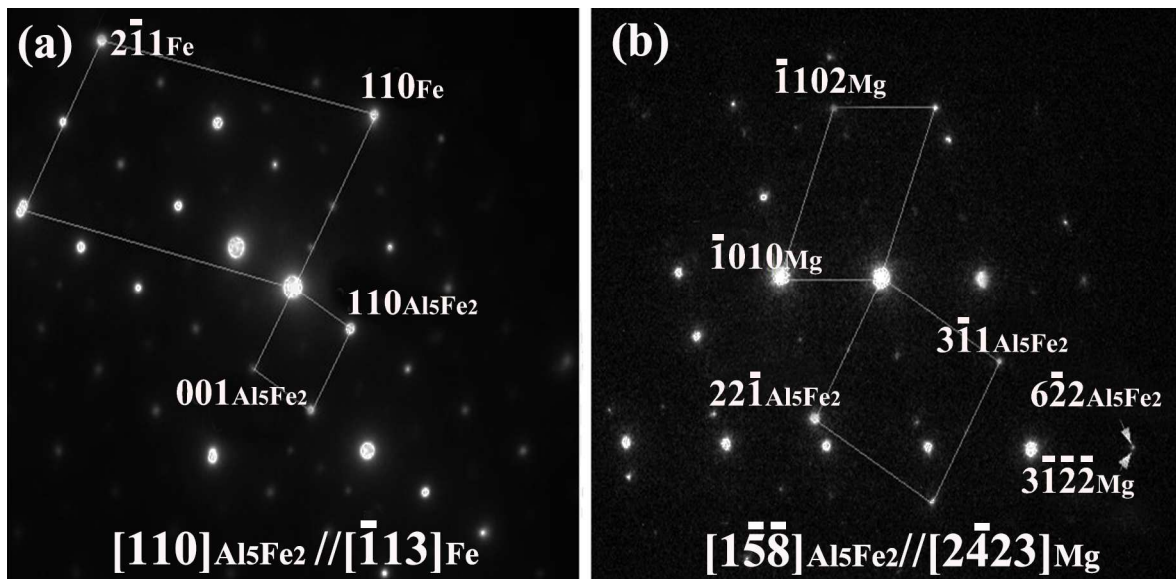
Fig. 4. XRD pattern of Zn-Al coated steel surface after etching by fuming HNO₃.



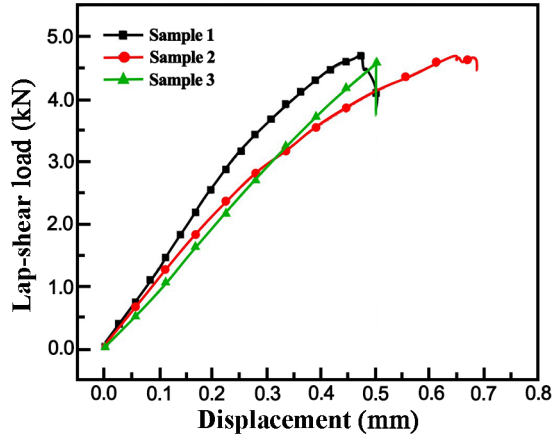
1
 2 **Fig. 5.** (a) Typical cross-section photograph of FSSW ZK60–steel joint using pinless tool, and
 3 microstructures and elemental line analyses of different zones in Fig. 5(a): (b) region B and (d)
 4 line D; (c) region C and (e) line E.



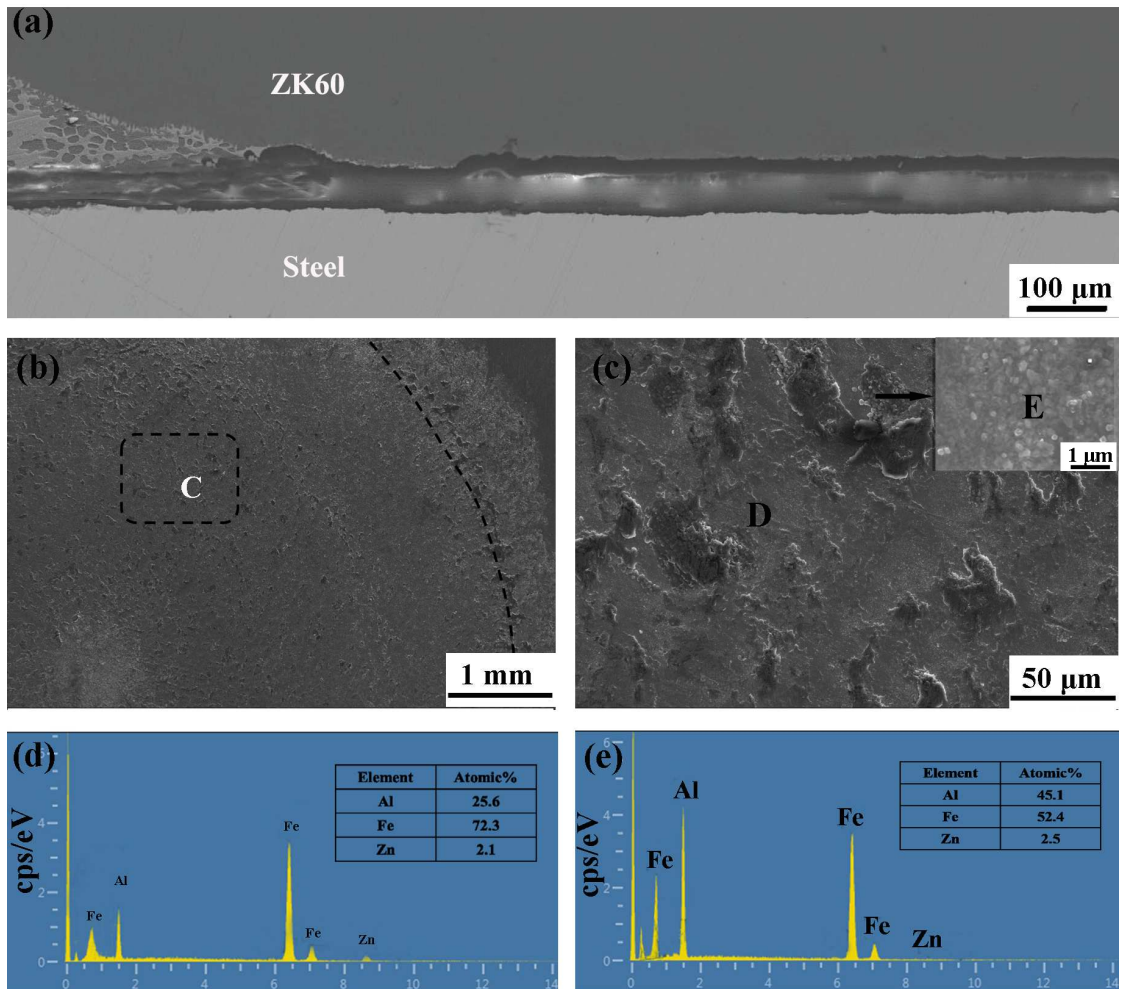
1
2 **Fig. 6.** (a) HAADF-STEM image of Mg-steel interface of FSSW ZK60-steel joint, (b)
3 elemental distribution of Mg, Fe, Zn and Al, (c) EDS spectra and (d) typical SADP obtained
4 from transition region in Fig. 6(a).



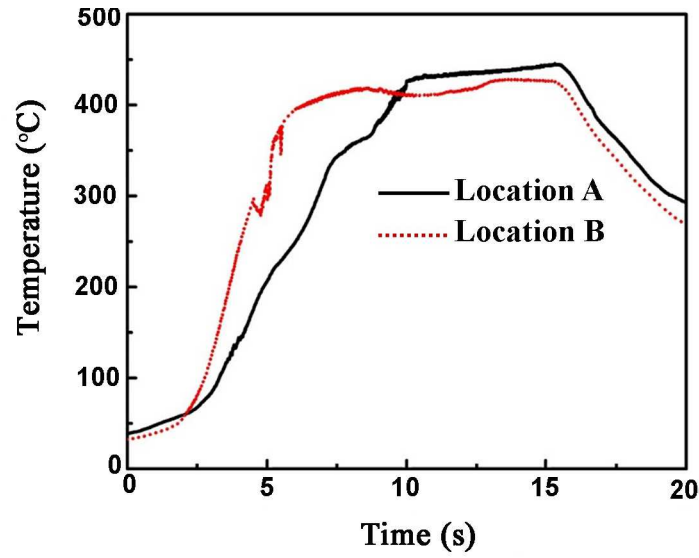
5
6 **Fig. 7.** Electron diffraction patterns taken from (a) $\text{Fe}_2\text{Al}_5/\text{Fe}$ and (b) $\text{Fe}_2\text{Al}_5/\text{Mg}$ interfaces,
7 with incident beam parallel to $[\bar{1}13]_{\text{Fe}}$ and $[110]_{\text{Al}_5\text{Fe}_2}$ in (a) and $[\bar{1}5\bar{8}]_{\text{Al}_5\text{Fe}_2}$ and $[\bar{2}4\bar{2}3]_{\text{Mg}}$ in (b),
8 respectively.
9



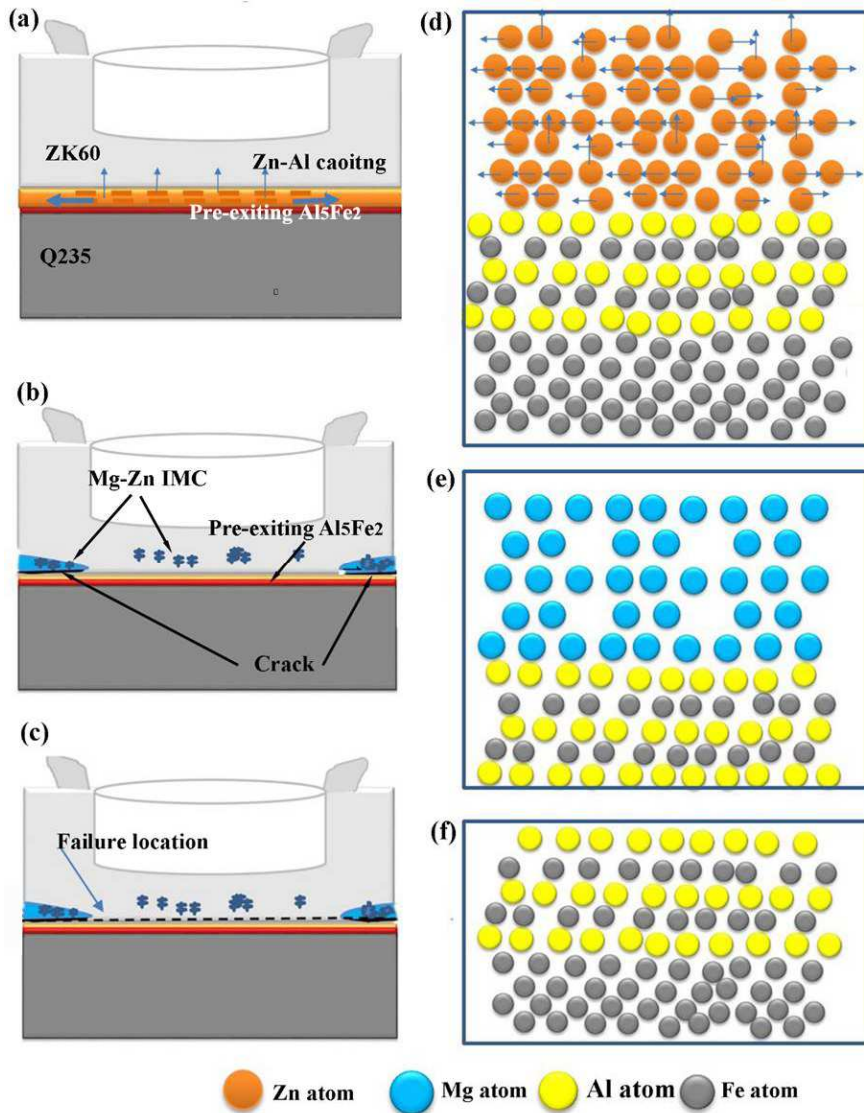
1
2 **Fig. 8.** Load-displacement curve of FSSW ZK60-steel joint.



3
4 **Fig. 9.** (a) Typical fracture location of FSSW ZK60–steel joint, (b) SEM image of fracture
5 surface and (c) magnified graphs of region C in Fig. 9(b) and EDS spectra obtained from (d)
6 region D and (e) region E in Fig. 9(c).
7



1
2 **Fig. 10.** Temperature profiles of locations A and B during FSSW of ZK60 and steel.



3
4 **Fig. 11.** Schematic of Zn-Al coating evolution of typical FSSW ZK60–steel joint: (a)

- 1 movement of Zn-Al coating; (b) formation of joint; (c) failure location; (d) movement of Zn
- 2 atom during FSSW; heterophase interfaces of (e) $\text{Fe}_2\text{Al}_5/\text{Mg}$ and (f) $\text{Fe}_2\text{Al}_5/\text{Fe}$ after FSSW.